9-1-2010

A Structural Dynamics Analysis of a Manduca Sexta Forewing

Travis W. Sims

Anthony N. Palazotto
Air Force Institute of Technology

Aaron G. Norris

A Structural Dynamic Analysis of a Manduca Sexta Forewing

Travis W. Sims[1], Anthony N. Palazotto[2] and Aaron Norris[3]

ABSTRACT

Micro air vehicles (MAVs) are intended for future intelligence, surveillance, and reconnaissance use. To adequately fulfill a clandestine capacity, MAVs must operate in close proximity to their intended target without eliciting counter-observation. This objective, along with DARPA's constraint of a sub-15 centimeter span, requires future MAVs to mimic insect appearance and flight characteristics. This paper describes an experimental method for conducting a structural analysis of a *Manduca Sexta* (hawkmoth) forewing. Geometry is captured via computed tomography (CT), and frequency data is collected using laser vibrometry in air and vacuum. A finite element (FE) model is constructed using quadratic beams and general-purpose shell elements, and an eigenanalysis is conducted. A preliminary verification of the FE model is carried out to ensure the *Manduca Sexta* forewing is adequately characterized, providing a basis for future fluid-structural interaction computations. Included is a study regarding the aeroelastic effects on flapping-wing insect flight, and an analysis of the structural dynamic anomalies of conventional, flat, semi-rigid flapping wings. Experimental tests revealed the first three modes of a clamped *Manduca Sexta* wing in vacuum are 86 Hz, 106 Hz, and 155 Hz; tests in air reveal a frequency shift of 26.5% from vacuum, indicating a possible aeroelastic contribution to frequency response. The finite element model produced first three modes of 84.6 Hz, 106.1 Hz, and 317.7 Hz, indicating that the model is limited to the second wing mode and lower frequencies. Possible sources of error include poor geometric modeling due to low CT resolution, inadequate modeling of camber, and inaccurate estimation of material properties.

NOMENCLATURE

ω_i = i^{th} natural frequency

1. INTRODUCTION

Over the course of last two decades, the demand for unmanned intelligence, surveillance and reconnaissance (ISR) assets has grown at an extraordinary pace. Physical separation of an aircraft and its human operator has provided unprecedented loiter times, range, low-cost compared to equivalent manned systems, and pilot safety. To supplement future ISR capabilities, many have proposed "micro" air vehicles (MAVs) that would revolutionize the field of remote sensing with their low cost, extreme maneuverability, and inconspicuous operation [11]. If successfully manufactured, the MAV of the future will be capable of a multitude of close-quarters reconnaissance tasks, ranging from battlefield operations to safety inspections of civilian structures. Table 1 outlines the Defense Advanced Research Projects Agency's (DARPA) vision for the MAV [11].

[1] Graduate student, Air Force Institute of Technology, Dept. of Aeronautics and Astronautics

[2] Professor, Air Force Institute of Technology, Dept. of Aeronautics and Astronautics

[3] Doctoral Candidate, Air Force Institute of Technology, Dept. of Aeronautics and Astronautics

Table 1. MAV Design Requirements [11]

Specification	Requirements	Details
Size	< 15.24 cm	Maximum Dimension
Mass	~ 100 g	Objective GTOW
Range	1 to 10 km	Operational range
Endurance	60 min	Loiter time on station
Altitude	< 150 m	Operational ceiling
Speed	15 m/s	Maximum flight speed
Payload	20 g	Mission dependent
Cost	$1,500	Maximum cost, 2009 USD

A brief look at any conventional flight-line reveals the stark contrast between current aircraft design and that of the proposed MAV. Today, all conventional, powered aircraft feature prominent engines with unnatural-looking wings. Moreover, a primary goal in wing design is maintaining structural integrity by reducing the magnitude of structural oscillations [1]. Even bounded harmonic responses – such as limit cycle oscillations – are avoided to circumvent material fatigue [8]. Turning to nature for insight into future MAV designs reveals a sharp departure from over a century of design practice: not only are insect wing oscillations permitted, they are abundant, highly-efficient, flight mechanisms [12].

Following in these biological footsteps, it is conceivable that future MAVs will be purposely designed with flapping wings, closely mimicking insect flight. This fundamental shift from quasi-rigid wings with separate power plants to a flexible airfoil integrates the generation of lift and thrust constitutes a dramatic change in design philosophy. Among other insects, the *Manduca Sexta*, or hawkmoth (see Figure 1) [1], serves as a blueprint from which engineers might learn important design criteria for MAVs. Within the context of this investigation, the *Manduca Sexta* is notable, since its size and capabilities are similar to DARPA's requirements in Table 1 [12].

Figure 1. An adult, female *Manduca Sexta* (Hawkmoth) [6].

Still, there are many questions that remain unanswered by previous work. Does the *Manduca Sexta* beat its wings near their natural frequencies? Is the hawkmoth's forewing a linear or nonlinear structure? Is the response dominated by inertial forces or aeroelastic effects – or both? What level of model sophistication is necessary to adequately represent biological wings? Asked another way, what simplifications could a manufacturer of synthetic *Manduca Sexta* forewings make to achieve structural characteristics similar to the biological wing? Answering these questions requires experimental and numerical analyses of the structural and fluid mechanics that dominate *Manduca Sexta* wings.

The objective of this work is to produce a finite element model of a *Manduca Sexta* forewing grounded in experimental vibration testing. In so doing, many of the above questions are addressed and answered, laying the foundation for future work. To this end, the natural modes (frequencies) and modeshapes of the hawkmoth forewings are identified via laser vibrometry. Testing is accomplished

in air and vacuum, to observe potential aeroelastic effects. Second, a finite element model capable of representing the observed modal behavior is developed and analyzed. Geometric dimensioning is accomplished via computed tomography (CT) imaging methods.

2. EXPERIMENTAL METHODS

2.1. Experimental Setup

Frequency analyses of a *Manduca Sexta* forewing were conducted using a Polytec PSV-400 scanning laser vibrometer. Wings were mounted into a foam-lined clamp, which was bolted to a motor. The motor was connected to an amplifier that received signals from the Polytec function generator. The motor and wing were encased in a transparent, acrylic vacuum, angled to prevent back-scatter to the laser head (see Figure 2). The wings were excited using a pseudo-random input, with frequencies up to 400 Hz. Time domain data was acquired with velocity decoders and converted to the frequency domain via the fast Fourier transform (FFT). During vacuum tests, the pressure was held constant at room temperature and approximately 530 Pa [3.98 Torr]. During tests in air, the vacuum chamber was closed, but kept at room temperature and pressure.

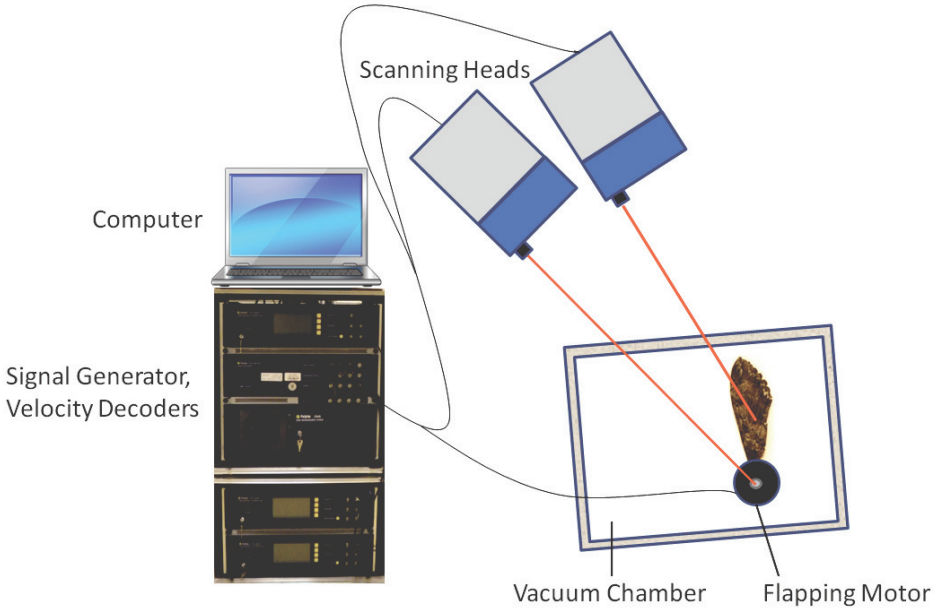

Figure 2. Schematic of experimental setup.

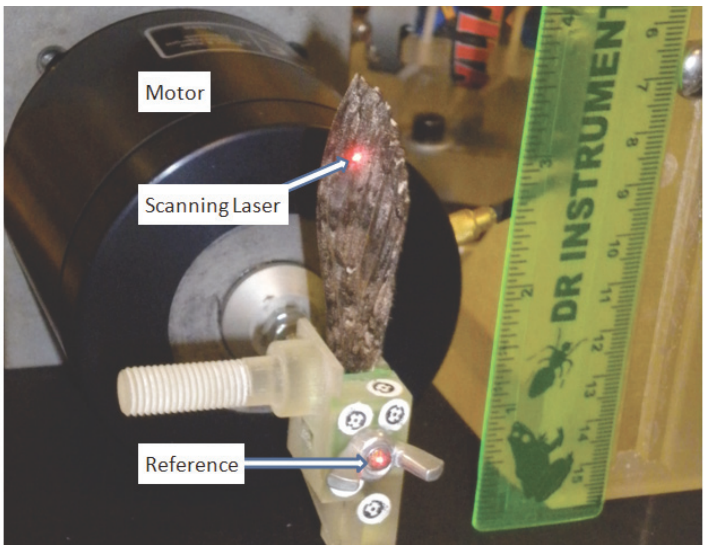

Figure 3. Wing motor and laser configuration used during testing.

Two laser heads were used while conducting frequency extraction tests. A reference laser focused on the bolt-head that held the wing clamp in place, while the other laser scanned the wing, as shown in Figure 3. The scanning laser followed a pre-set pattern of scan points over the surface of the wing. During the tests, the motor flapped the wing at very low amplitudes[4], to minimize any aeroelastic influence that might not be present during normal operation by the *Manduca Sexta*. To ensure no ambient air leaked into the vacuum during testing, a digital pressure gage was attached to the vacuum, and monitored during testing.

2.2. Wing Preparation

The *Manduca Sexta* wings were removed scalpel by making an incision along the root (see Figure 4); great care was taken to avoid damaging the wing prior to testing. Observed during this process was a natural camber in the *Manduca Sexta* forewing, that was flattened when placed inside the motor clamp[5]. This change in wing geometry imposes internal stress which in turn alters the natural frequencies and mode shapes of the wing – an unacceptable result in a noninvasive experimental method. To circumvent this unnatural flattening of the wing, polymeric foam paint was applied inside the clamp on both sides of the wing, as shown in Figure 5. Frequency tests of homogeneous, isotropic beams were conducted and compared to the published analytical solution [10] to verify the clamped boundary condition.

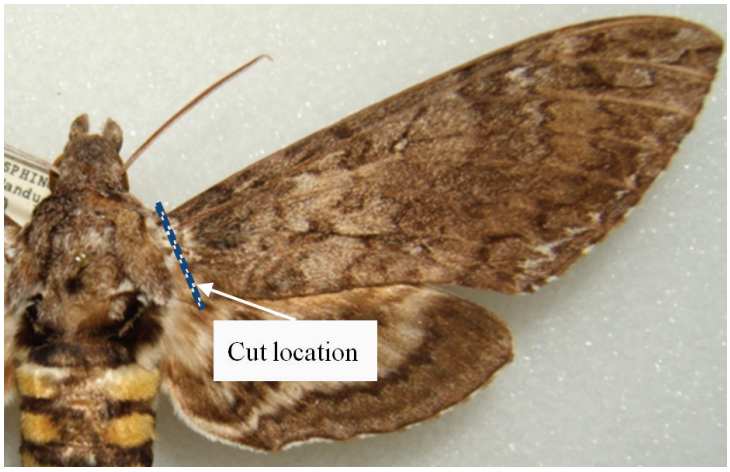

Figure 4. Cut location during wing removal [6].

Figure 5. Side view of a clamped *Manduca Sexta* forewing (a), and the foam-lined clamp of cross-section A-A (b). The four symbols shown in (a) are reference points for future photo-modeling use.

[4] While not quantified, these amplitudes were small enough that they were barely visible with the naked eye.

[5] Note that this camber is not constant during flight, as with man-made wings [16]. The present work considers structural characteristics only for the static wing.

2.3. Computed Tomography (CT) Imaging

The *Manduca Sexta* forewing is a highly complex structure. There are a multitude of veins and membranes, many of which intersect multiple times. Because of this complexity, a high-fidelity geometric model is required to proceed with any finite element efforts. One apparatus (among others) that is capable of characterizing this geometry is a computed tomography (CT) "scanner." Computed tomography scanners rotate an imager around a specimen, while taking a series of X-ray images. These two-dimensional images are then post-processed to build a three-dimensional digital model [7].

2.3.1. Imaging a Manduca Sexta Wing

A freshly removed wing was clamped, as shown in Figure 5, and placed inside the CT imager. Figure 6 shows the *Manduca Sexta* forewing, with only high-density structures visible. Note that in this image, the inner and outer diameters of the veins are clearly visible upon close inspection, and the boundary between vein and membrane is easily distinguishable. Perhaps one of the most obvious artifacts of only resolving the higher-density structures is the noticeable lack of membrane tissue. It appears that the wing skin is of equal density at all points, possibly indicating homogeneity – casting doubt on previous assertions of varying material properties [1, 4, 9].

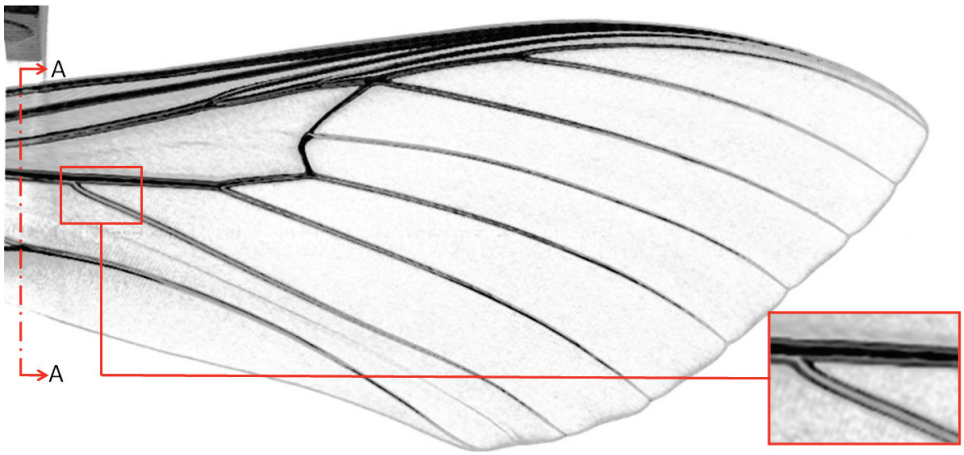

Figure 6. Processed CT image of a female *Manduca Sexta's* right forewing, showing a prominent vein structure.

2.3.2. Wing Geometry

A total of 16 cross-sectional images were obtained by digitally "slicing" the CT model; one such cross-section is shown in Figure 7. Consisting of a total of five veins, the image illustrates the complexity of the *Manduca Sexta* vein structure – no two veins are alike, though all are approximately circular. Furthermore, the vein closest to the trailing edge (right-most in Figure 7) is dramatically different than the others at this particular cross-section location (Figure 6, A-A). Here, two veins are merging into one, larger vein.

Figure 7. Cross-section A-A (see Figure 6) from a *Manduca Sexta* wing, approximately 2 mm. from the root. The prominent left vein is the leading edge.

2.4. MODAL IDENTIFICATION OF A MANDUCA SEXTA FOREWING IN VACUUM

A *Manduca Sexta* forewing was analyzed using a scanning laser vibrometer to determine its frequency content. As described previously, the frequency data were collected *in vacuo*, to eliminate any potential aeroelastic effects. The frequency response function and coherence plots for this case are shown below, in Figure 8 and Figure 9. Table 2 gives the first three natural frequencies observed in this experiment.

Table 2. Natural frequencies of a Manduca Sexta forewing in vacuum.

	Frequency, Hz[6]
ω_1	86 ± 2
ω_2	106 ± 2
ω_3	155 ± 2

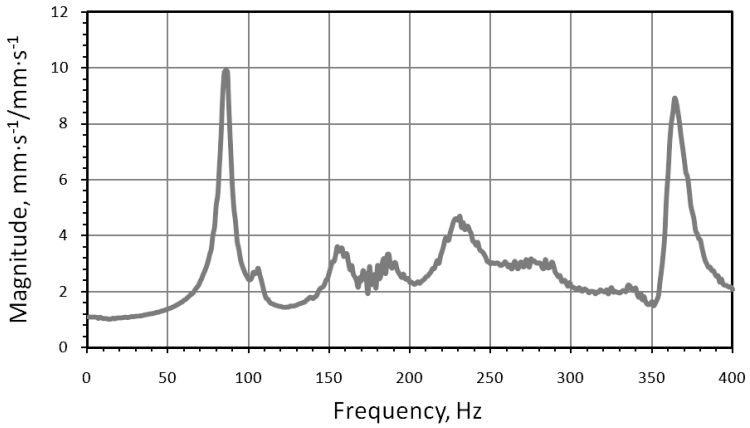

Figure 8. Frequency response function (magnitude) for a *Manduca Sexta* wing in vacuum.

Notice that the coherence decreases as the frequency approaches the 400 Hz cutoff. Since this analysis is primarily concerned with only the first three modes, the reduction of coherence values at high-frequencies does not negatively impact the fidelity of the low-frequency (less than 250 Hz) measurements. These high coherence values seem to indicate that the wing is a linear structure, since any structural response is strongly correlated to its excitation[7].

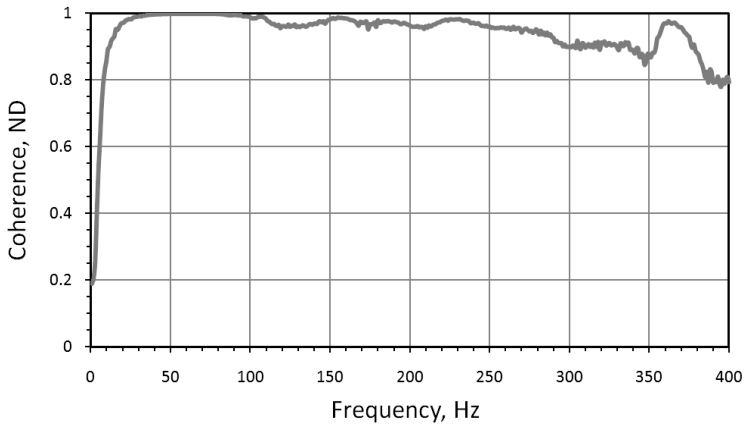

Figure 9. Spectral coherence for the Manduca Sexta wing analysis.

[6] For the duration of this document, uncertainty values are based on manufacturer specifications unless otherwise specified.

[7] Included in this structural linearity is the presence of any stress-stiffening effects on frequency response. For the present boundary conditions these effects are either negligible or implicitly captured by this method.

Although every continuous structure has an infinite number of natural frequencies, [10] considering only the first three modes is sufficient for the purposes of this analysis. Previous research indicates that the *Manduca Sexta* beats its wings at approximately 25 Hz. [16], thus it is unlikely that higher modes have more than miniscule effects on the wing's operating deflection shape. It is therefore likely that the first three modes are dominant in characterizing the action of the *Manduca Sexta* forewing.

The modeshapes – how the structure responds to a natural frequency input – are important parameters in describing the wing[8]. Due to the orthogonality of the eigenvalues and eigenvectors, each of the natural frequencies (modes) listed in Table 2 has a unique, associated modeshape [10]. The modeshapes corresponding to the first three natural frequencies are shown below.

The first modeshape (86 Hz, Figure 10) behaves much like the first bending mode of a cantilevered beam: the wing flaps in only one plane of motion, with a maximum displacement at the tip. By contrast, the second mode (106 Hz, Figure 11) is similar to the first torsional mode of a plate fixed at one end. The maximum displacement is at the wing tip, with the leading and trailing edges deflecting asynchronously. Also akin to the second mode of a plate fixed at one end (first torsion), the second modeshape of the hawkmoth wing rotates about a central axis, approximately located at the half-chord[9] line.

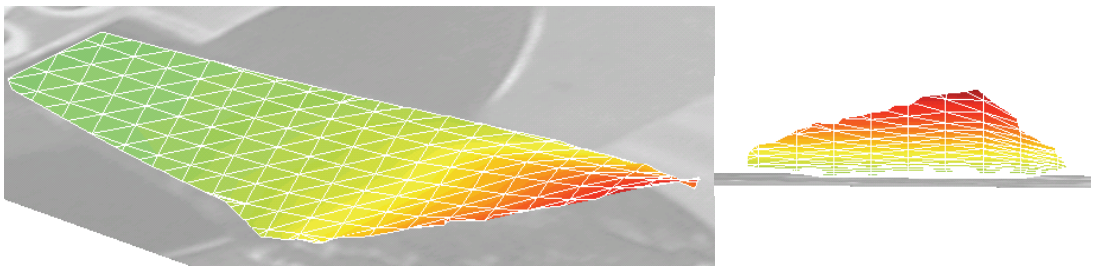

Figure 10. First modeshape (86 Hz) of a *Manduca Sexta* wing, shown from an isometric view (a) and a tip view (b).

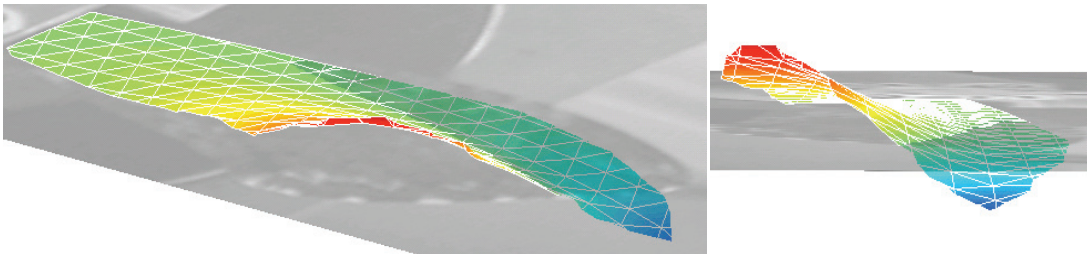

Figure 11. Second modeshape (106 Hz) of a Manduca Sexta wing, shown from an isometric view (a) and a tip view (b).

The third mode occurs at 155 Hz (Figure 12). In many ways, the behavior of the wing at this frequency is similar to that of its second mode, with an important exception. Instead of asynchronous flapping about the half-chord line, this mode displays synchronous (in-phase) flapping of the leading and trailing edges at the tip. As this occurs, the half-chord line exhibits bending similar to the first-beam bending mode, but out of phase with the flapping in the leading and trailing edges. The combination of the leading / trailing tip flapping and half-chord bending creates an overall deflection shape resembling a saddle. This "saddle mode" is shown below, in Figure 12.

[8] It should be noted that the term "modeshape" is used here to denote an operational deflection shape that is strongly dominated by the wing response at resonance .

[9] The wing chord is defined as a line connecting the leading and trailing edges of an airfoil [1].

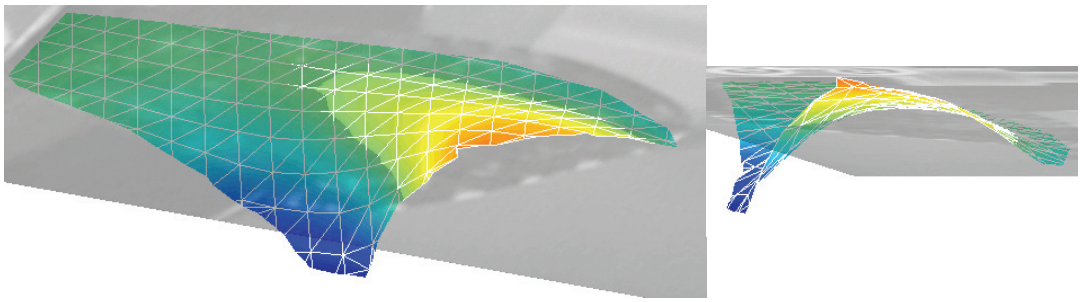

(a) (b)

Figure 12. Third modeshape (155 Hz) of a Manduca Sexta wing, shown from an isometric view (a) and a tip view (b).

2.5. Modal Identification of a Manduca Sexta Forewing in Air

The previous experiment was repeated with a fresh wing, this time in air and vacuum.[10] The modeshapes of the wing were the same as those given above; however the frequencies at which they occurred were different. Evidently, the fluid-structural interaction serves as a damping mechanism in air, reducing the frequency content by as much as 26% in the lower modes. Likewise, the ratios of the natural frequencies changed, and seemed to scale with increasing frequency. This finding is indicative of a possible aeroelastic coupling due to the strong influence of viscosity at low Reynolds numbers. Table 3 lists the frequencies associated with each mode, and Table 4 compares the frequency ratios. Note that the frequency values for the wings given in Tables 2 and 3 are different, but the ratio of their first and second modes are nearly identical. This unlikely coincidence is documented in Ref [13].

Table 3. Natural frequencies of a *Manduca Sexta* wing in air and vacuum.

	Air, Hz	**Vacuum, Hz**	**Change,%**
ω_1	59 ± 2	80 ± 2	26.3 ± 1.6
ω_2	75 ± 2	98 ± 2	23.5 ± 1.1
ω_3	95 ± 2	118 ± 2	19.5 ± 0.7

Table 4. Comparison of frequency ratios of Manduca Sexta and wing in air and vacuum.

	Air, Hz	**Vacuum, Hz**	**Change,%**
ω_2/ω_1	1.28 ± 0.08	1.23 ± 0.05	3.6 ± 0.5
ω_3/ω_1	1.62 ± 0.09	1.48 ± 0.06	8.8 ± 1.3

2.6. Paper Wing Tests

In light of the camber observed during the computed tomography (CT) scans, one wonders whether camber is an important structural characteristic of the hawkmoth wing. Certainly, it is a widely accepted fact that camber increases low-Reynolds number aerodynamic efficiency [14] – a valuable attribute for small wings. However, to date, flat, rigid wing designs with homogeneous material account for a large number of MAV research [12]. These wings provide computational simplicity, and are cost effective – thus it may prove beneficial to know whether a flat, homogeneous wing reasonably approximates the actual forewing. To explore the extent to which the veins and membranes are quasi-isotropic, and the degree to which camber effects the hawkmoth wing modeshapes, a paper wing of the same planform was constructed. Figure 13 shows the wing used, and the results of this test are shown in Figure 14.

[10] The first wing, discussed previously, underwent CT imaging before the frequency analysis in vacuum. Repeating the study in air with the same wing would have allowed the wing sufficient time to dry, thus altering its response.

Figure 13. Paper wing used in frequency experiments.

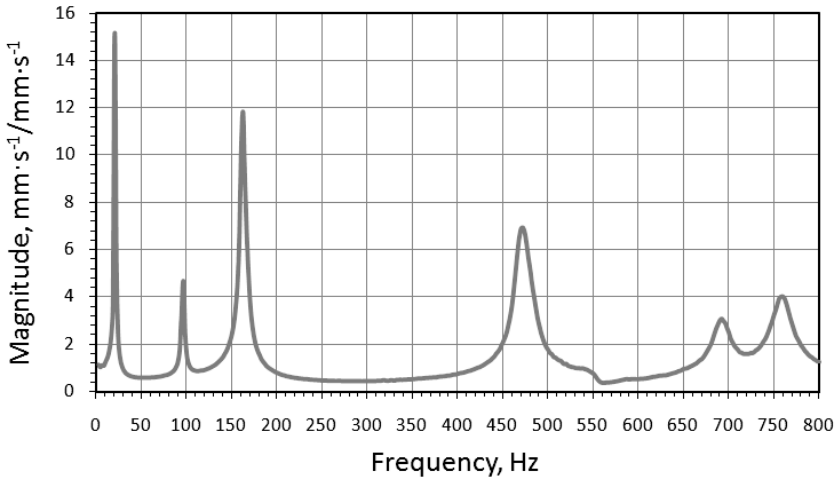

Figure 14. Frequency response function of the paper wing.

Table 5 compares the ratios of the natural frequencies obtained during the paper wing tests to those of the *Manduca Sexta* in vacuum. Clearly, the two are unrelated in their frequency content, and for reasons other than their difference in materials and mass. While one might expect different natural frequencies, the hawkmoth wing and paper wing would have similar frequency ratios if material properties and mass were their only differences.

Although at different frequencies and a different frequency ratio, the first two modeshapes of the paper wing are nearly identical to those of the hawkmoth. The first mode is a flapping mode, similar to a homogeneous fixed-free beam's first bending mode (see Figure 15). The second modeshape is similar to the second mode of a flat, rectangular plate fixed at one end: it exhibits torsion about the central axis, from root to tip (see Figure 16). The third mode is a second bending mode not seen in the *Manduca Sexta* wing (see Figure 17); the fourth mode appears to be a saddle mode with strong tip deflection, also not seen in the *Manduca Sexta* wing (see Figure 18).

Table 5. Comparison of frequency ratios of *Manduca Sexta* and paper wings in vacuum.

	***Manduca Sexta* Wing**	**Paper Wing**
ω_2/ω_1	1.23 ± 0.05	4.8 ± 0.58
ω_3/ω_1	1.48 ± 0.06	8.1 ± 0.91
ω_4/ω_1	2.17 ± 0.08	23.6 ± 2.46
ω_5/ω_1	2.69 ± 0.09	34.6 ± 3.56

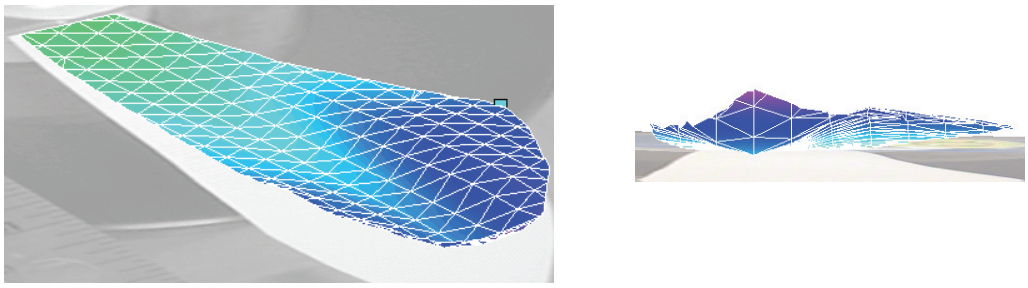

(a) (b)

Figure 15. First modeshape (20 Hz) of a paper *Manduca Sexta* wing, shown from an isometric view (a) and a tip view (b).

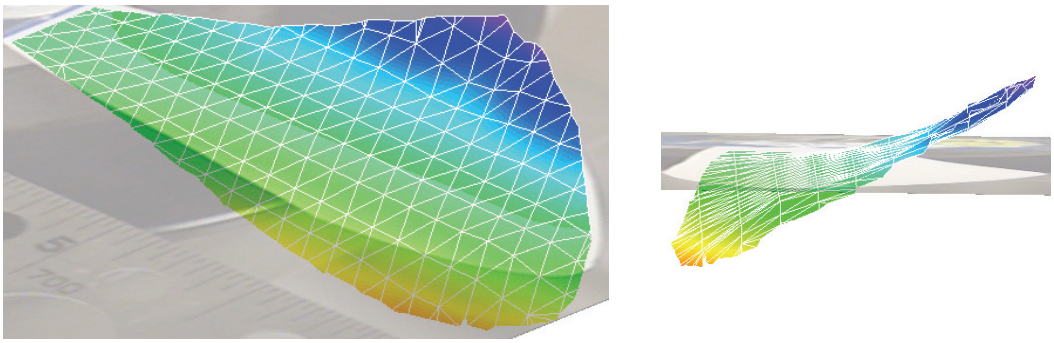

(a) (b)

Figure 16. Second modeshape (96 Hz) of a paper *Manduca Sexta* wing, shown from an isometric view (a) and a tip view (b).

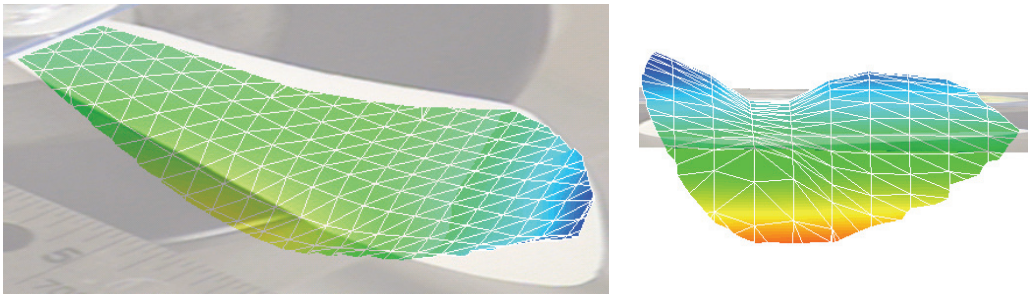

(a) (b)

Figure 17. Third modeshape (162 Hz) of a paper *Manduca Sexta* wing, shown from an isometric view (a) and a tip view (b).

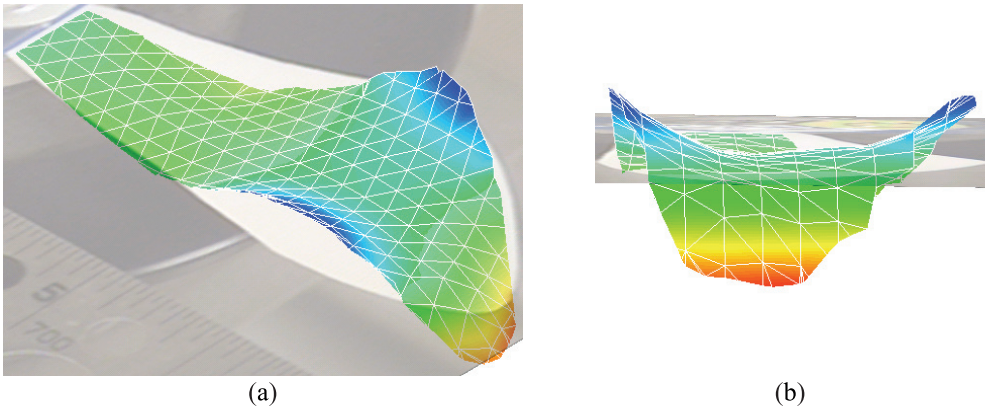

(a) (b)

Figure 18. Fourth modeshape (472 Hz) of a paper *Manduca Sexta wing*, shown from an isometric view (a) and a tip view (b).

Comparing the actual *Manduca Sexta* wing and the flat, paper specimen gives insight regarding the importance of the wing components. The hawkmoth wing appears to be dominated by plate-like modeshapes – as one might expect given its dimensions. By contrast, the paper wing seems to exhibit a composite beam / plate behavior, intermittently resembling either structure. The absence of the second beam bending mode from the *Manduca Sexta* wing and the lack of tip motion in the saddle mode suggests the veins have structural importance – that is, they are not only useful as circulatory members.

3. NUMERICAL METHODS

The paper wing experiment demonstrated that a flat, homogeneous airfoil does not adequately represent a *Manduca Sexta* forewing (at least from a structural dynamics standpoint). In an effort to understand the relative importance of camber and venation in the design space, two parametric studies were conducted: the effect of camber variation on frequency content is studied using a FE model of a wing with no venation pattern; second, a flat wing with a venation pattern typical of a *Manduca Sexta* is studied to determine the frequency effect of varying vein diameters. In each case, the robustness of the selected elements was evident from a convergence study that showed virtually no change with mesh refinement[11]. All finite element models were developed using Abaqus Standard[12].

3.1. Camber Effects

A finite element wing with the same platform as the *Manduca Sexta* forewing was meshed using four-noded, doubly-curved, reduced-integration shells (six degrees of freedom per node[13], Koiter-Sanders formulation). The wing was cambered with a constant curvature representative of the curvature observed in the *Manduca Sexta* wing. Nine hundred elements[14] covered the cambered wing during the frequency analysis. In order to make a direct comparison to the flat wing model, the material properties of paper were used during the cambered analysis[15]. For comparison, the frequency results for the flat and cambered (13 %c)[16] cases are given below, in Table 6. By examining the results of both cases, one immediately finds that the curvature of the wing dramatically increases its stiffness.

Table 6. Comparison of natural frequencies of flat and cambered wing FE solutions, using general-purpose shell elements (S4R).

	Flat Wing, Hz	**Cambered Wing, Hz**
ω_1	22	159
ω_2	109	173
ω_3	159	797

The first three modeshapes of the cambered wing analysis are given in the figures below. The first modeshape, shown in Figure 19, differs slightly from that of the flat wing. Although the wing is still displacing in a fashion reminiscent of classical first bending, a large portion of the movement is now seen in along the trailing edge instead of at the tip. The second modeshape, however, appears to be similar in many respects to the deformations of the flat wing. Here, torsion is the primary driver, though the axis of rotation also seems to have shifted slightly towards the trailing edge. The third modeshape (Figure 21) presents the most striking evidence camber's effect on the wing. Here, the third mode is of a saddle shape, similar to the third mode of the actual *Manduca Sexta* forewing. Despite this similarity, the large midside deflections in the leading and trailing edges of the model are not seen in the *Manduca Sexta* wing; this difference further highlights the important stiffening effect of the veins.

[11] Largest change of any mode was 1.5 Hz when the mesh was refined from 348 elements to 4,121

[12] Abaqus is a registered trademark of the Simulia Corporation.

[13] S4R in the Abaqus vernacular

[14] The mesh density was determined though an extensive convergence study.

[15] Properties were experimentally determined to be E = 7.5 MPa, ν = 0.3, $\rho = 8.6\text{x}10^{-7}$ [15].

[16] Invoking the standard nomenclature, the camber is the maximum distance between the chord line and the "mean camber line" – the locus of all points halfway between the upper and lower airfoil surfaces – normalized by the chord length (%c) [1].

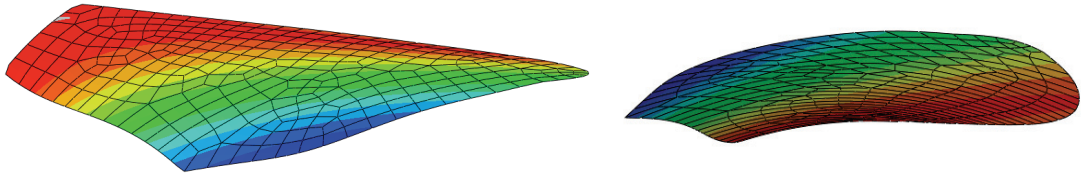

(a) (b)

Figure 19. First modeshape (159 Hz) of a cambered, FE wing, shown from an isometric view (a) and a tip view (b).

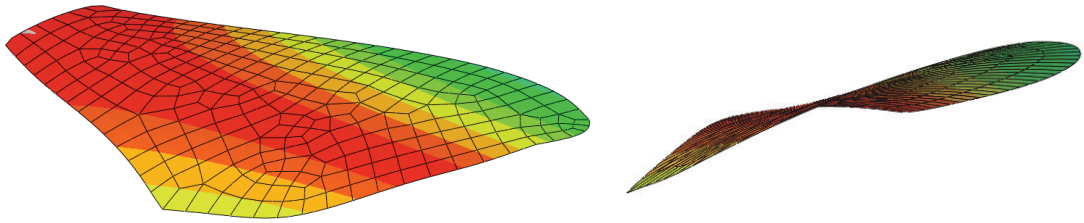

(a) (b)

Figure 20. Second modeshape (173 Hz) of a cambered, FE wing, shown from an isometric view (a) and a tip view (b).

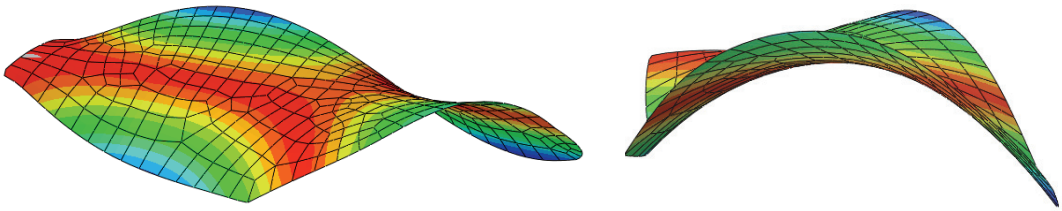

(a) (b)

Figure 21. Third modeshape (797 Hz) of a cambered, FE wing, shown from an isometric view (a) and a tip view (b).

The preceding study of camber effects on natural frequency was repeated for several values between zero and 15º (13% of chord)[17]. The same homogeneous, isotropic wing meshed with general-purpose shells was used. The results are plotted below, in Figure 22. The first natural frequency increases linearly with camber, while the second mode, also increasing, is substantially less affected by a change in camber. The third mode has the unique distinction of changing modeshapes during this analysis. At low camber values (less than 4.5% chord), the third modeshape is the second bending mode observed previously in flat wings. Above the cutoff value of 4.5% of chord, the camber-induced stiffness eliminates the second bending mode. Here, the saddle mode experiences a negative frequency shift, and becomes the third mode observed in the *Manduca Sexta* wing. It is notable that the second bending and saddle modes do not experience a mode reversal at high camber values. Instead, the second bending mode simply disappears – or changes shape so dramatically that it can no longer be characterized as "second bending." Regardless of the modeshape presented, the third mode is strongly affected by even slight changes in camber.

[17] The camber in the *Manduca Sexta* wing varies from 0 %c to approximately 20%c, with an average of approximately 13 %c.

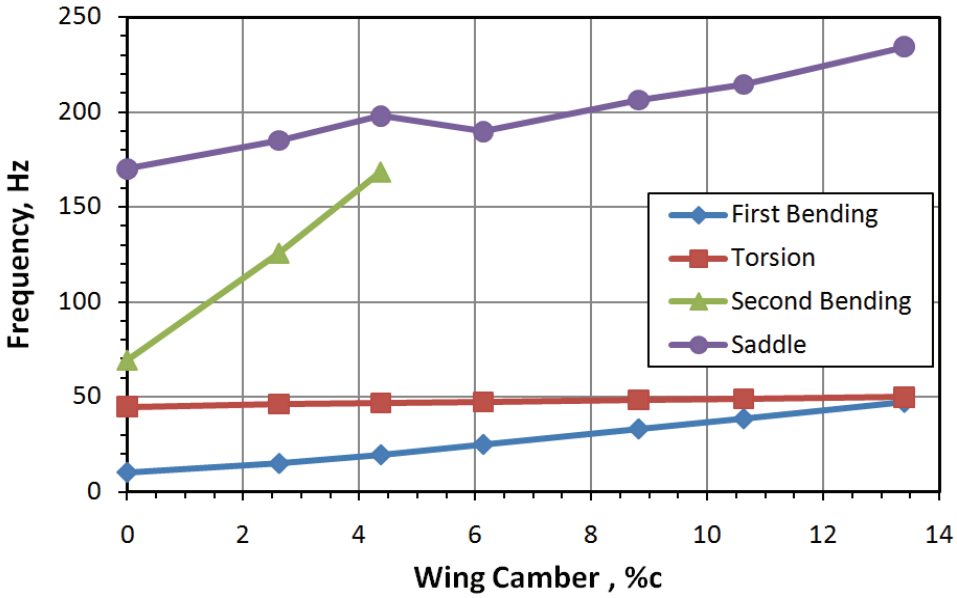

Figure 22. Effects of camber on natural frequency in a homogeneous Manduca Sexta wing.

3.2. Vein Effects

A flat wing model with included was devised consisting of three-noded quadratic beams (B32) and four-noded shells (S4R), representing the veins and membrane tissue, respectively. Both the beam and the shell elements have six degrees of freedom per node. The beams (veins) are prismatic, each having a unique cross-section. Cross sectional properties of each vein were averaged using the CT measurements. The membrane (denoting tissue, not an element type) is also of constant thickness (0.12 mm) at all points[18]. The three-noded quadratic beam (B32) and membrane sections (four-noded general purpose shell, type S4R) were tied together, enforcing continuity of displacement and rotation among beam and shell elements. Figure 23 shows the assembly used during analysis.

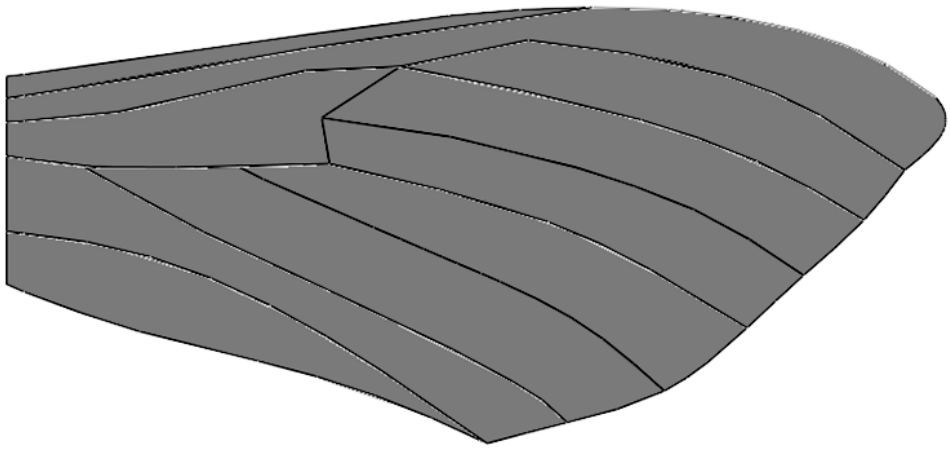

Figure 23. Assembly of vein (quadratic beam) and membrane (Koiter-Sanders shell) sections.

To date, no work has been published on the material properties of the *Manduca Sexta*; however, follwing their work with the *Tibicen Canicularis* (cicada), Mengesha, Vallance, Barraja and Mittal published material property values for that species [9].

[18] Very little variation in membrane thickness was observed during the CT scans.

Table **7** gives the reported values for the cicada wing, obtained through a nano-indentation procedure. Note that the thickness of the cicada membrane is close to that of the *Manduca Sexta* – a heartening result.

The Young's modulus of the membrane is greater than that of the veins in the cicada wing. This result is not surprising, since many entomologists have noted that there are two basic classes of insect wings: stiff and flexible. The *Tibicen Canicularis* (cicada) is of the order *Hemiptera*, and has a rigid wing [9], while the *Manduca Sexta* has a flexible wing, as do most insects in the order *Lepidoptera* [16]. As a result, the initial hawkmoth model constructed in Abaqus uses the material properties of the *Tibicen Canicularis*, with the elastic moduli interchanged: the hawkmoth veins are assumed to be stiffer than its membrane.

Table 7. Material properties of a *Tibicen Canicularis* (cicada) reported by Mengesha, Vallance, Barraja, and Mittal [9].

	Veins	**Membrane**
Mass Density, g/c,m-3.	2.30	2.30
Young's Modulus, GPa	1.90	3.70
Poisson's Ratio	0.495	0.495
Thickness, μm		12.20

Table 8. Natural frequencies of a flat Manduca Sexta wing model

	Frequency, Hz
ω_1	41
ω_2	2. 91
ω_3	225
ω_4	308

The wing shown in Figure 23 was meshed with three-noded quadratic beams (B32), and four-noded general-purpose shells (S4R). A Lanczos method eigenvalue solver was used to compute the modes and modeshapes of the first three modes. The natural frequencies obtained from this analysis are given above in Table 8.

The modeshapes of the flat *Manduca Sexta* wing model are shown in the figures below. By now, the first two modeshapes are familiar; the planform dictates first bending and torsion at the first and second modes, respectively. The third modeshape shows some deviation from the flat paper wing and its model. Instead of the deformations resembling pure second-bending seen previously, the beams influence the modeshape to add significant flattening near the tip. Still, the third modeshape has many aspects that appear similar to second-bending, and is not seen experimentally in the *Manduca Sexta* wing.

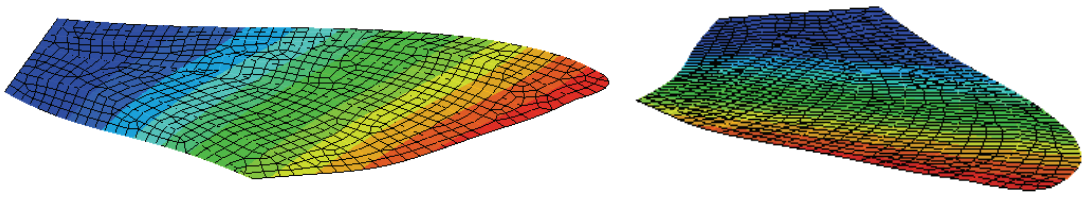

(a) (b)

Figure 24. First modeshape (41 Hz) of a flat, FE wing with added veins, shown from an isometric view (a) and a tip view (b). Color bands denote displacement.

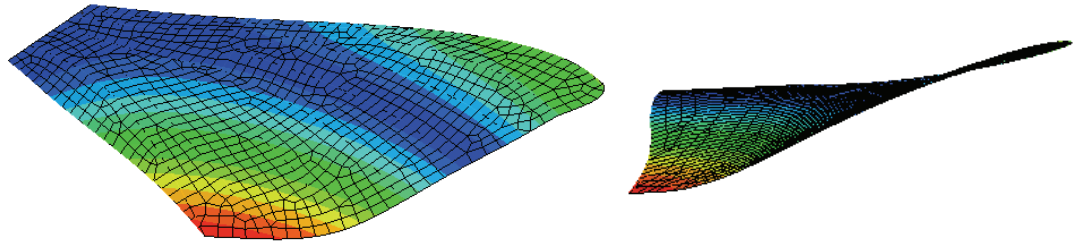

(a) (b)

Figure 25. Second modeshape (92 Hz) of a flat, FE wing with added veins, shown from an isometric view (a) and a tip view (b). Color bands denote displacement.

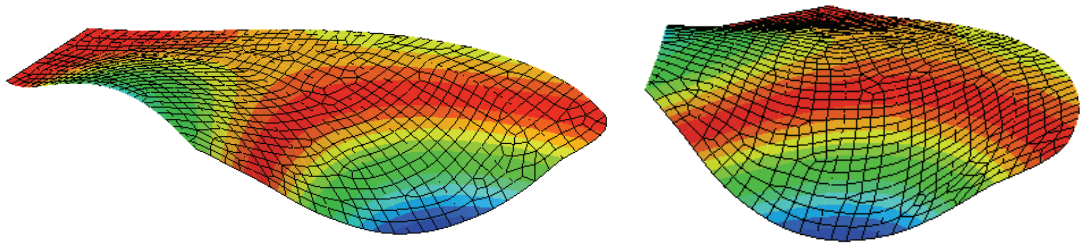

(a) (b)

Figure 26. Third modeshape (225 Hz) of a flat, FE wing with added veins, shown from an isometric view (a) and a tip view (b). Color bands denote displacement.

The fourth modeshape is shown below, in Figure 27, and is similar to the saddle mode seen above. Adding the vein (beam) structure has shifted the central axis toward the trailing edge, and they are now nearly parallel. Accompanying the axis shift is a more prominent tip deflection than previously observed. Also notable is the lack of midsection motion in the leading and trailing edges, resembling the *Manduca Sexta* more than previous models. The midsection stiffness and the presence of the third (extra) mode not seen in the cambered model are indicative that both venation and camber are important structural characteristics.

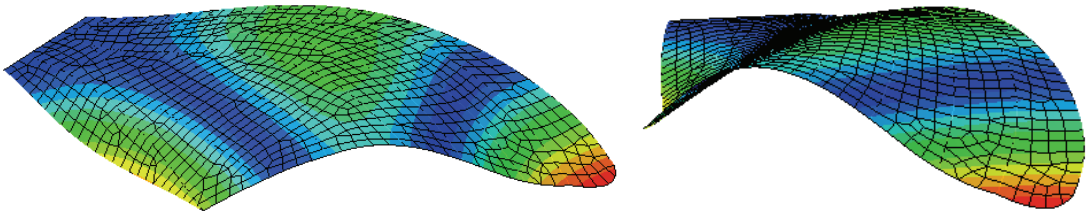

(a) (b)

Figure 27. Fourth modeshape (308 Hz) of a flat, FE wing with added veins, shown from an isometric view (a) and a tip view (b).

Using the flat wing model shown in Figure 23, a study of the effects of vein thickness on natural frequency was conducted. In this study, a vein thickness factor was defined as a coefficient that acted uniformly on all veins (*e.g.*, a thickness factor of two doubled the diameter of all veins). Throughout this study, a refined, converged mesh was held unchanged, using quadratic beams and general-purpose shell elements to model the veins and membranes, respectively. Based upon the previous assertion that the *Manduca Sexta* has a flexible wing structure, the material properties of *Tibicen Canicularis* veins and membrane were again reversed. The results of the vein thickness study are plotted in Figure 28.

Examining the results of the frequency vs. vein thickness plot reveals a common theme: the first two natural frequencies increase nearly linearly with vein stiffness (via diameter), and at the same rate; conversely, the third mode is strongly affected by vein thickness (thus stiffness). The third modeshape is a second bending mode at low stiffness values, and the fourth mode is a saddle mode. Increasing the vein diameter beyond 120% of the measured values causes the second bending mode to disappear; when this occurs, the saddle mode experiences a reduction in frequency and becomes the third mode.

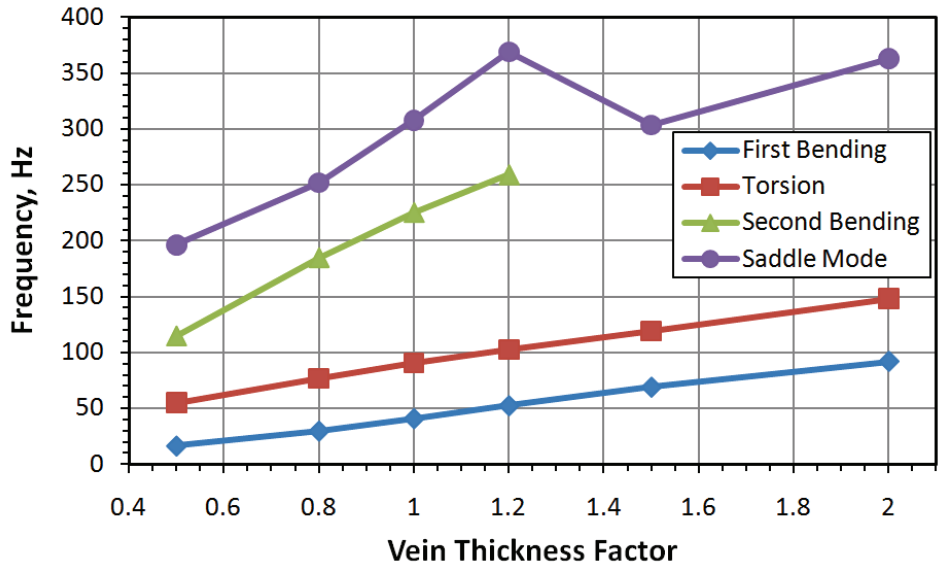

Figure 28. Natural frequency as a function of vein thickness for a flat wing, using reversed *Tibicen Canicularis* material properties. A vein thickness of 1 is equivalent to the average measured value for each individual vein. Average vein radii vary from 0.07 mm to 0.6 mm.

It should be noted that the preceding investigations involve estimated material properties and a wide range of camber and vein dimensions that reveal a possible non-uniqueness of modal solutions. Indeed, structural stiffness, *EI*, is a combination of material property and moment of inertia effects, in which an inadvertent underestimation of one contributing factor may be compensated for by a corresponding overestimation of another. With Young's modulus, Poisson's ratio, and density estimated (but unknown), and geometric measurements limited by the resolution of the CT scans, producing a validated structural model of a *Manduca Sexta* may be possible, albeit non-unique.

4. NUMERICAL RESULTS AND DISCUSSION

The previous FE studies reveal that the natural frequencies of the *Manduca Sexta* wing are strongly correlated to camber and vein thickness. Consequently, both camber and vein thickness variation as a function of span were included in the finite element model. It was also assumed (without verification[19]) that the material properties of the *Manduca Sexta* are reasonably close to those of the *Tibicen Canicularis*.

4.1. Model Construction

Reflecting the results of the CT imaging process, the membrane tissue was modeled as a shell of constant thickness. Conversely, vein profiles varied with span, also reflecting cross-sectional measurements. Each of the vein (beam) cross-sections change discontinuously at unique spanwise locations, since no two veins are alike. Between each of the section locations, an average value of vein thickness was computed, and a new section was created when the vein thickness varied by more than 10% from the average section value. Figure 29, below, shows the *Manduca Sexta* wing model color-coded by cross-section. All beams are tied at the midsection of the shells (membrane tissue), enforcing continuity of displacement and rotation.

[19] Preliminary nano-indentation studies place the Young's modulus of dry, aged *Manduca Sexta* wings between 2 and 5 GPa. Material properties for the veins have yet to be determined.

In light of the previous studies asserting that the *Manduca Sexta* wing is far more flexible than the *Tibicen Canicularis* wing, the material properties used mirrored the reversed cicada properties.[20] Table 9 shows the material properties used during model construction. During the experimental portion of this endeavor, over 50 wings were weighed, with an average forewing mass of 0.0416 grams, with a standard deviation of 0.0037 grams. In comparison, the Abaqus-determined model mass of is 0.040 grams, well within one standard deviation of the average *Manduca Sexta* wing mass.

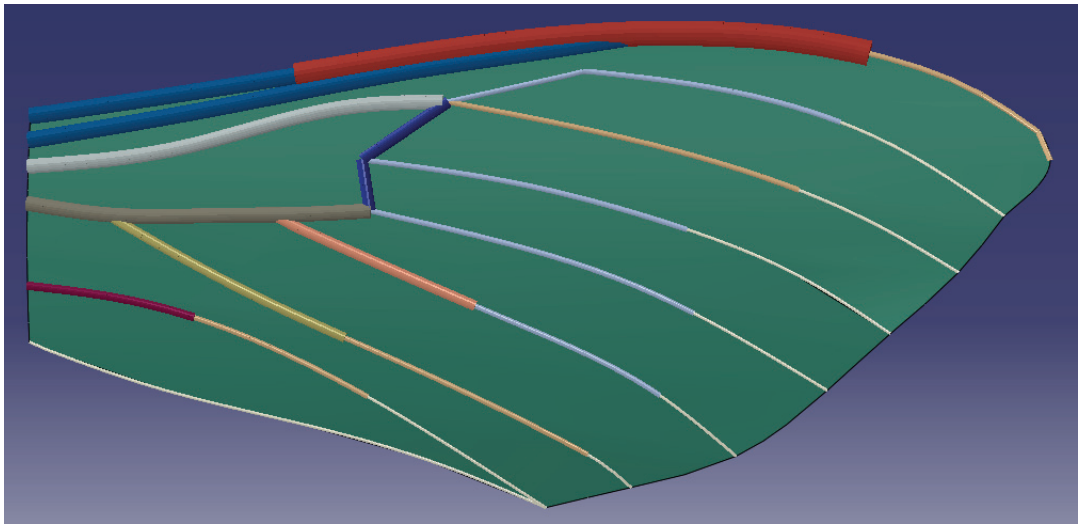

Figure 29. Planform view of a finite element model of a *Manduca Sexta* forewing, color coded by cross-section dimension.

Table 9. Assumed values of material properties for a Manduca Sexta (hawkmoth) wing.

	Veins	Membrane
Density, g/c,m-3.	2.30	2.30
Young's Modulus, GPa	4.00	1.90
Poisson's Ratio	0.495	0.495
Thickness, μm		12

4.2. Frequency Analysis Results

The wing model shown in Figure 29 was meshed with three-noded quadratic beams and four-noded, doubly-curved, shells, using a reduced integration formulation of 11 through the thickness integration points. The first three natural frequencies of this model (converged values) are presented in Table 10, and compared to the experimentally obtained values of the *Manduca Sexta* forewing.

Table 10. Natural frequency results of a *Manduca Sexta* FE model, and comparison to experimental values.

	Experimental, Hz	FE Model, Hz	Minimum Difference
ω_1	86 ± 2.00	84.60	0.00%
ω_2	106 ± 2.00	106.10	0.00%
ω_3	155 ± 2.00	317.70	102.40%

[20] Preliminary nano-indentation tests validate this assumption, see Note 11.

Table 11. Comparison of frequency ratios of *Manduca Sexta* and FE wings.

	Experimental, Hz	FE Model, Hz	Minimum Difference
ω_2/ω_1	1.23 ± 0.05	1.25	0.00%
ω_3/ω_1	1.80 ± 0.07	3.91	100.80%

It is immediately obvious that the first two natural frequencies of the *Manduca Sexta* wing and the finite element model match very well, as does their ratio. The finite element model does not adequately match the third mode, however. The predicted third natural frequency and its ratio to the first mode differs from experimental values by a factor of roughly two. As previous studies have shown, the third mode is the most sensitive (of the three modes considered) to stiffness effects resulting from camber, cross-sectional shape, and material property variation.

Not surprisingly, the first two modeshapes of the finite element model correlate well with the experimental results seen in the *Manduca Sexta* wing. The first modeshape of the finite element wing is plotted below, in Figure 30[21]. This modeshape is the familiar first bending mode, with color bands denoting magnitude of displacement. As seen experimentally in the *Manduca Sexta* wing, the wing displacement is a function of span, with little variation in the chordwise direction.

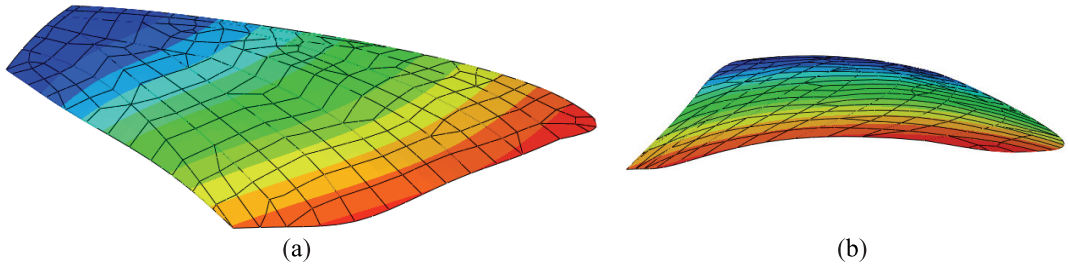

Figure 30. First modeshape (84.6 Hz) of FE *Manduca Sexta* wing model, shown from an isometric view (a) and a tip view (b).

The second modeshape is a torsional mode, and is plotted in Figure 31. Unlike the torsional modes seen previously, the second modeshape of this model does not affect the wing in a rigid, plate-like fashion. That is, instead of the entire wing (or a majority of it) rotating as a single, planar unit about a central axis, the wing of Figure 31 shows significant curvature in the tip view. This deflection is consistent with the second modeshape of the *Manduca Sexta* wing, shown in Figure 11. In both cases, the central axis, about which the rotation occurs, is offset slightly forward of the half-chord line. Moreover, the finite element model accurately predicts that the vertical displacement of the trailing edge has a slightly greater magnitude than that of the leading edge.

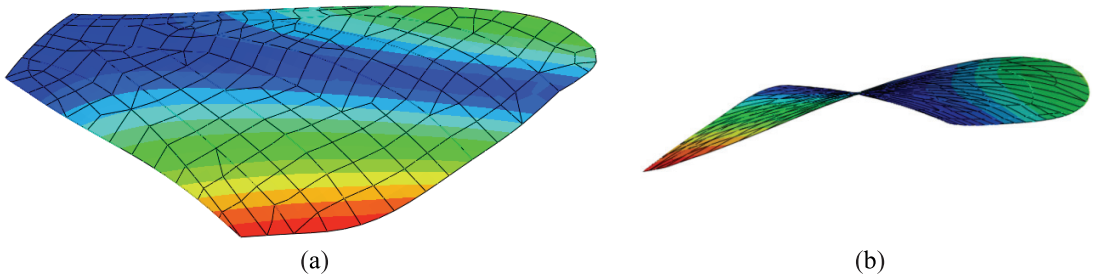

Figure 31. Second modeshape (106.1 Hz) of FE *Manduca Sexta* wing model, shown from an isometric view (a) and a tip view (b).

[21] For readability's sake, the most refined (converged) mesh is not shown in the figures. The converged mesh contains so many elements that the color bands denoting displacement are no longer visible due to the black outline of the elements.

The third modeshape is a saddle-mode, shown below, in Figure 32. Although the frequency value predicted by the finite element model does not coincide with the 155 Hz value observed in the hawkmoth wing, its modeshape is stunningly similar. Like the saddle mode shown in Figure 12, the finite element model predicts a smooth deflection of nearly constant radius from the tip view. Likewise, the chordwise deflection is angled, so that the axis of rotation is slightly off center, giving the trailing edge the greatest magnitude of deflection in the vertical direction. This effect causes the trailing edge slope to be greater than that of the leading edge; as a result, the root is visible in the upper left corner of Figure 32 (b) – mimicking the *Manduca Sexta's* response in Figure 12 (b). Convergence studies were carried out to ensure accuracy of the finite element solutions. Mesh sizes between 295 and 80,633 elements were investigated, during which a converged solution was achieved with approximately 2,500 elements.

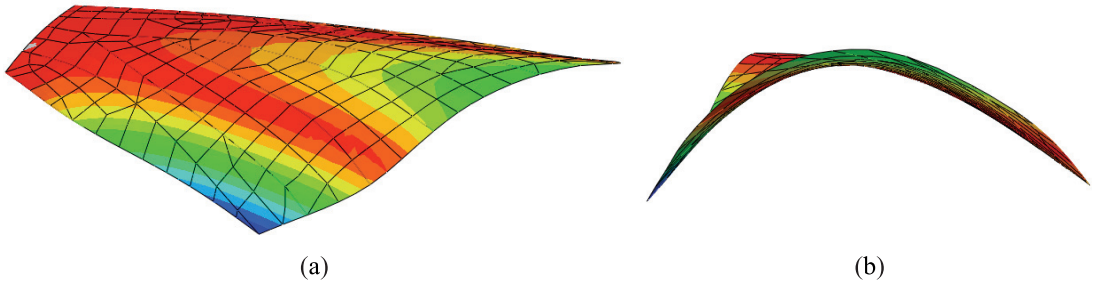

Figure 32. Third modeshape (317.7 Hz) of FE *Manduca Sexta* wing model, shown from an isometric view (a) and a tip view (b).

4.3. Model Limitations

Before undertaking a numerical analysis of the *Manduca Sexta* wing, one of the stated objectives was to develop a finite element model capable of adequately representing the first three natural frequencies and their associated modeshapes. The above results indicate that the finite element model produced acceptable results for the first two frequencies and modeshapes. While the third modeshape appears qualitatively similar to the saddle mode observed in the *Manduca Sexta* wing experiment, the frequency values are different by approximately a factor of two. There are several possible reasons why this deviation might exist: low resolution during component dimensioning, inadequate characterization of wing camber, and poor estimation of material properties. Each of these possibilities is explored below.

4.3.1. Component Dimensioning

The dimensions of the vein and membrane structures were obtained via computed tomography (CT) measurements. During this process it was observed that the vein dimensions (and to a lesser extent the membrane thickness) are a function of span. As the cross-section location moves from root to tip the veins taper, and the low resolution of the CT imager prohibits accurate measurement. Figure 33 compares images of the first three veins (leading edge is to the left) at the wing root, and approximately the half-span location (20 mm from the root). Due to the change in vein dimensions, the differences in image quality are striking. Gone from the half-span image is the clear inner-diameter, and the separation of the first two veins is indistinguishable.

Figure 33. Comparison of first three veins at the wing root (a) and 20 mm (approximately half-span) from the root (b). In both cases, the leading edge is to the image left.

Figure 33(b) highlights the effect of decreasing the vein diameter at constant image resolution: the relative importance of a single pixel is dramatically elevated. The pixel size is the limiting value of precision in digital image measurement, thus attempting to dimension structures with length scales of the same order of magnitude as the pixel size greatly increases the probability of measurement errors. The trend observed in Figure 33 continues as the cross-section location advances toward the tip. As the veins taper, they become less visible, and finally appear to blend into the membrane prior to their terminal locations.

Comparing the results of the vein thickness (diameter) studies to the results of the finite element model of the *Manduca Sexta* wing suggests the outer diameter of the veins may have been overestimated. The higher-quality CT images near the wing root reveal that the veins are surrounded by a coating of membrane tissue. As the cross-section location moves from root to tip, the relative thickness of the membrane coating increases due to a corresponding decrease in vein thickness.

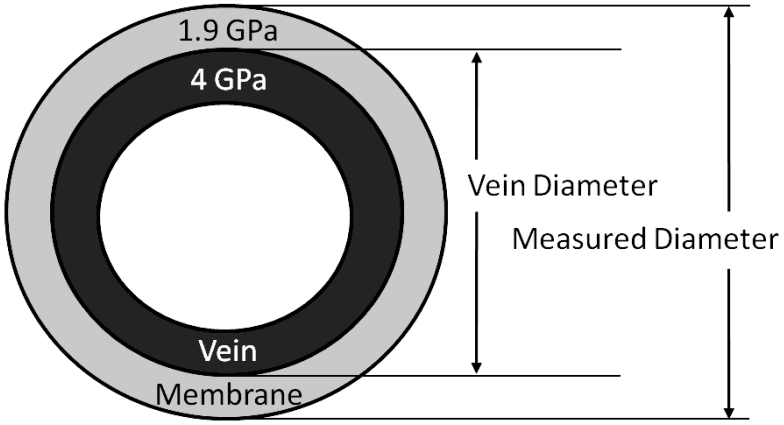

Figure 34. Schematic of membrane tissue surrounding the vein. Low CT resolution results in measuring the outer-diameter of both structures, instead of the vein only.

It is likely that low CT image quality resulted in measuring the total diameter of what appeared to be the vein structure, instead of dimensioning only the vein and excluding the surrounding membrane (see Figure 34, above). Since the assumed value of Young's modulus of the veins (beams) was more than twice that of the membrane tissue (shells), measuring the *total* diameter surrounding the vein would result in a significant stiffening effect. Conversely, because the veins and membrane are assumed to be of the same density, over-measuring the vein diameter would not increase the mass of the model – making measurement errors more difficult to detect. Thus, if a more accurate model is to be produced, a geometry measurement technique that offers higher resolution than the CT imager is necessary.

4.3.2. Modeling Camber

The approach taken during the finite element modeling process was to model the wing with a shell of constant radius and thickness. The selected camber was an average value based on CT measurements, and was measured using the NACA wing standard: the maximum distance between the chord line and the mean camber line is the camber value. The curvature of a *Manduca Sexta* wing is far more complex than that of wings typical of man-made designs. Instead of the smooth wing surface of constant concavity seen in most commercial wing designs, the *Manduca Sexta* wing is of positive concavity near the leading edge, and negative concavity over the majority of the wing surface, as shown in Figure 7. Additionally, the camber is a function of span in the *Manduca Sexta* wing. Future modeling efforts should include this geometric sophistication if high-frequency modes are to be matched.

4.3.3. Material Properties

After an exhaustive literature search of approximately 400 papers, no material properties for the *Manduca Sexta* (or monarch butterfly, a similar species of the order *Lepidoptera*) were found, leaving one forced to estimate Young's modulus, Poisson's ratio, and density during the modeling process. As a result, the material properties used in the finite element model were based on those of the *Tibicen*

Canicularis (cicada), as reported by Mengesha, Vallance, Barraja and Mittal [9]. The cicada is of the order *Hemiptera*, a class of species observed to have stiff, semi-rigid wings; conversely, the *Manduca Sexta* (hawkmoth) is of the order *Lepidoptera*, and is known to have more flexible wings than *Hemipterae* [9]. Based on this knowledge, the assumption that the Young's modulus of the *Manduca Sexta* wing components is likely the reverse of the *Tibicen Canicularis* was made.

Stiffness is a function of Young's modulus, geometry, and mass-density. While the mass of the finite element model was representative of what one might expect from a typical *Manduca Sexta* wing, it is possible that the agreement with the first two experimental modes was the result of the non-uniqueness of the stiffness value. The fact that the natural frequencies of the finite element model agree with the experimental results only in the first two modes likely indicates some total stiffness error in the model. Indeed, a fundamental concept in vibration theory is the effect of density and stiffness on frequency. A more accurate finite element model of the *Manduca Sexta* will likely require one to obtain material properties for the hawkmoth.

5. CONCLUSIONS

A structural dynamic analysis of a *Manduca Sexta* (hawkmoth) forewing was conducted in air and vacuum using laser vibrometry techniques. The first three modeshapes were presented and compared to those of a flat, homogeneous, isotropic paper wing. These tests showed a negative frequency shift of approximately 23% for same-wing modes in air and vacuum, indicating the presence of some aeroelastic coupling. Comparison of the *Manduca Sexta* wing to a paper wing of the same planform indicated that the venation present in the hawkmoth serves both a circulatory and structural role.

Using a homogeneous, isotropic shell model of the same planform as the *Manduca Sexta* wing, a parametric study of the effect of camber on natural frequency was conducted. During this study, all modes except the torsional mode were observed to be strongly dependent on camber-induced stiffness, indicating that camber is an important structural property of the *Manduca Sexta* wing. A similar parametric study of the effects of vein thickness on natural frequency was conducted, using a flat wing model with ten different prismatic beams. During this analysis, all modes were observed to be strongly correlated to vein thickness. Together, these studies reinforce the notion that without adequately capturing the geometry of the wing, creating a validated structural model may prove exceedingly difficult.

A finite element model of a *Manduca Sexta* wing was produced to accurately predict the first two natural frequencies and modeshapes as seen in the experimental data. The third modeshape is qualitatively similar to that observed in the *Manduca Sexta* wing, though the frequency values differ by a factor of approximately two. The agreement of the first two natural frequencies of the experimental wing and finite element model suggest that the model is useful for characterizing frequencies up to and including the second mode only. Further research is required to determine the importance of the experimental and numerical disagreement seen in the third and higher natural frequencies.

Comparing the model to the parametric studies of camber and vein diameter versus natural frequency suggest more precise modeling is required. While it is possible to model a more accurate distribution of camber using the CT images, the resolution is not sufficient to accurately measure vein profiles. It is strongly recommended that higher resolution imaging techniques be investigated if accuracy beyond the second mode is required.

The views expressed in this document are those of the author and do not reflect the official policy or position of the United States Air Force, Department of Defense, or the United States Government. This material is declared a work of the U.S. Government and is not subject to copyright protection in the United States.

REFERENCES

[1] Anderson, J. D., *Fundamentals of Aerodynamics*, 4th Ed., McGraw-Hill, 2007.

[2] Blisplinghoff, R. L., Ashley, H., & Halfman, R. L., *Aeroelasticity*, Addison-Wesley, 1955.

[3] Combes, S. A., & Daniel, T. L., "Flexural Stiffness In Insect Wings I. Scaling And The Influence Of Wing Venation", Journal of Experimental Biology, 2003, Vol. 206, pp. 2979-2987.

[4] Combes, S. A., & Daniel, T. L., "Flexural Stiffness In Insect Wings II. Spatial Distribution And Dynamic Wing Bending", *Journal of Experimental Biology*, 2003, Vol. 206, pp. 2989-2997.

[5] Gogulapati, A., Friedmann, P.P., Shyy, W., "Nonlinear Aeroelastic Effects in Flapping Wing Micro Air Vehicles", 49th AIAA/ASME/ASCE/AHS/ASC Structures, Structural Dynamics, and Materials Conference, 2008, AIAA-2008-1817.

[6] Hanrahan, S., Photo of a *Manduca Sexta*, Texas A&M University, Department of Entomology, 2006.

[7] Herman, G. T., *Fundamentals of Computerized Tomography*, 2nd Ed., Springer, 2009.

[8] Hodges, D. H., and Pierce, G. A., *Introduction to Structural Dynamics and Aeroelasticity*, Cambridge, 2002.

[9] Mengesha, T. E., Vallance, R. R., Barraja, M., and Mittal, R., "Parametric Structural Modeling of Insect Wings," *Bioinspiration and Biommetics*, 2009.

[10] Meirovitch, L., *Fundamentals of Vibrations*, McGraw-Hill, 2001.

[11] McMichael, J. M., and Francis, M. S., "Micro Air Vehicles – Toward a New Dimension in Flight," *Unmanned Systems*, 1997, Vol. 15, No. 3, pp.8-17.

[12] Michelson, R. C., and Reece, S., "Update on Flapping Wing Micro Air Vehicle Research," 13th Bristol International RPV Conference, 1998.

[13] Norris, A., Palazotto, P., & Cobb, R., *Structural Dynamic Characterization of an Insect Wing: Toward the Development of "Bug Sized" Flapping-Wing Micro Air Vehicles*, AIAA 2010-2790.

[14] Raymer, D. P., *Aircaft Design: A Conceptual Approach*, 4th Ed., AIAA Education Series, 2006, pp. 620-636.

[15] Sims, T. W., *A Structural Dynamic Analysis of a* Manduca Sexta *Forewing*, Master's Thesis, AFIT/GA/ENY/10-M22, http://handle.dtic.mil/100.2/ADA517375, 2010.

[16] Willmott, A. P., and Ellington, C. P., "The Mechanics Of Flight In The Hawkmoth Manduca Sexta, I. Kinematics Of Hovering And Forward Flight", *Journal of Experimental Biology*, 1997, Vol. 200, No. 21, pp. 2705-2722.

[17] Zienkiewicz, O. C., and Taylor, R. L., *The Finite Element Method for Solid and Structural Mechanics*, 6th Ed., Butterworth-Heinemann, Elsevier, 2006.